A novel LiDAR-GNSS-INS Two-Phase Tightly Coupled integration scheme for precise navigation

Mengchi Ai[1], Ilyar Asl Sabbaghian Hokmabad[2], Mohamed Elhabiby[3], Naser El-Sheimy[4]

[1]Dept. of Geomatics Engineering, University of Calgary, Calgary, Canada -mengchi.ai@ucalgary.ca ,
[2]Dept. of Geomatics Engineering, University of Calgary, Calgary, Canada ilyar.aslsabbaghianh@ucalgary.ca,
[3]Micro Engineering Tech. Inc., Calgary, AB, Canada, elhabiby@microengineering.ca
[4]Dept. of Geomatics Engineering, University of Calgary, Calgary, Canada -elsheimy@ucalgary.ca

Keywords: GNSS/INS navigation, Factor graph optimization, Extended Kalman Filter, LiDAR, Sensor fusion, IMU.

Abstract

Recent advances in precise navigation have extensively utilized the integration of Global Navigation Satellite System (GNSS) and Inertial Navigation System (INS), particularly in the domain of intelligent vehicles. However, the efficacy of such navigation systems is considerably compromised by the reflection and multipath disruptions of non-light-of-sight (NLOS) signals. Light Detection and Ranging (LiDAR)-based odometry, an active perception-based sensor known for its precise 3D measurements, has become increasingly prevalent in augmenting navigation systems. Nonetheless, the assimilation of LiDAR odometry with GNSS/INS systems presents substantial challenges. Addressing these challenges, this study introduces a two-phase sensor fusion (TPSF) approach that synergistically combines GNSS positioning, LiDAR odometry, and IMU pre-integration through a dual-stage sensor fusion process. The initial stage employs an Extended Kalman Filter (EKF) to amalgamate the GNSS solution with IMU Mechanization, facilitating the estimation of IMU biases and system initialization. Subsequently, the second stage integrates scan-to-map LiDAR odometry with IMU mechanization to support continuous LiDAR factor estimation. Factor graph optimization (FGO) is then utilized for the comprehensive fusion of LiDAR factors, IMU pre-integration, and GNSS solutions. The efficacy of the proposed methodology is corroborated through rigorous testing on a demanding trajectory from an urbanized open-source dataset, with the system demonstrating a notable enhancement in performance compared to the state-of-the-art algorithms, achieving a translational Standard Deviation (STD) of 1.269 meters.

1. Introduction

With the development of smart vehicles, the capability of the real-time positioning and navigation has become critical and fundamental requirement (Ai et al., 2022). Given considerations of extensive coverage and cost efficiency, GNSS/INS systems equipped with low-cost receivers and Micro-Electro Mechanical Systems (MEMS)-level IMU have traditionally been the cornerstone of vehicle positioning technology (Moussa et al., 2021). Nevertheless, these systems are prone to significant drift, particularly when navigating urban environments characterized by signal reflectance and dynamic objects. The amalgamation of GNSS solutions with INS mechanization, which can ameliorate accuracy by leveraging continuous pose data, has garnered increasing interest among researchers in recent years (Chiang et al., 2020).

Literature in this field delineates two solutions pertaining to GNSS/INS sensor fusion: the filter-based algorithms, and optimization-based algorithms. Filter-based odometry solutions, such as Kalman filter and its derivatives, iteratively update the vehicle's new pose based on its preceding state (Chiang et al., 2019). These methods are validated in published research works, demonstrating that a continuous state can be deduced by computing nonlinear transformation matrices. In contrast, optimization-based approaches utilize the branch of data and optimize the all the measurements and state via a nonlinear solver. Research work (Wen et al., 2021) has shown that the utilization of FGO can achieve promising navigation results, notwithstanding drifting errors instigated by GNSS outliers. Moreover, research by (Wang et al., 2021) demonstrate that the FGO solution shows the capability on fusing heterogeneous measurements and constraints (e.g., loop closure constraints and primitive constraints). However, in the absence of supplementary measurements, the pure GNSS/INS navigation solution is unable to self-correct, particularly in the face of adverse GNSS conditions and satellite insufficiency. Consequently, the integration of GNSS/INS systems with perception-based sensors, like Light Detection and Ranging (LiDAR), which can furnish relative local pose data, has emerged as a viable alternative.

With the advantages of unsensitive to various illumination and the accurate range measurements, an increasing number of researches focus on how to integrate the LiDAR-based odometry (LO) or map-aided LiDAR localization with GNSS/INS system, within the FGO framework. For example, studies in (Liu et al., 2023; Shan et al., 2020) integrates the LiDAR measurements, GNSS signals and IMU measurements in loosely or tightly coupled system by comprehensively eliminating the distance errors. Studies in (Ai et al., 2023) introduce the map matching constraints to the navigation system which can highly eliminate the translation errors in the vertical direction. However, current solutions can't prevent the positioning drifting from utilizing all the measurements at one single stage optimization. Specifically, the limitations of the current solutions can be discussed as the following two aspects:

(1). *The system's initialization accuracy is limited:* Initialization's aim is to estimate the parameters affected by noise, such as bias and scale factor, and to ascertain the direction of gravity. Especially when the initial speed is low, the accuracy of IMU measurements is affected by the noisy, resulting in drifting at the initial stage.
(2). *Susceptibility to local minima:* Contemporary methodologies often merge all measurable data and states within a singular back-end framework, which can be compromised by noise and outliers. A single estimator's failure can precipitate system-wide drift due to the local minima encountered by nonlinear solvers. Additionally, while most navigation systems are dependent on the LiDAR-Inertial odometry (LIO) estimator for continuous estimation, the GNSS solution is relegated to providing a global absolute constraints. Consequently, in scenarios where the GNSS data is compromised by unreliable observations, the system is still prone to substantial errors.

To address the mentioned challenging issues, this paper proposes a novel two-phase sensor fusion strategy that integrates GNSS,

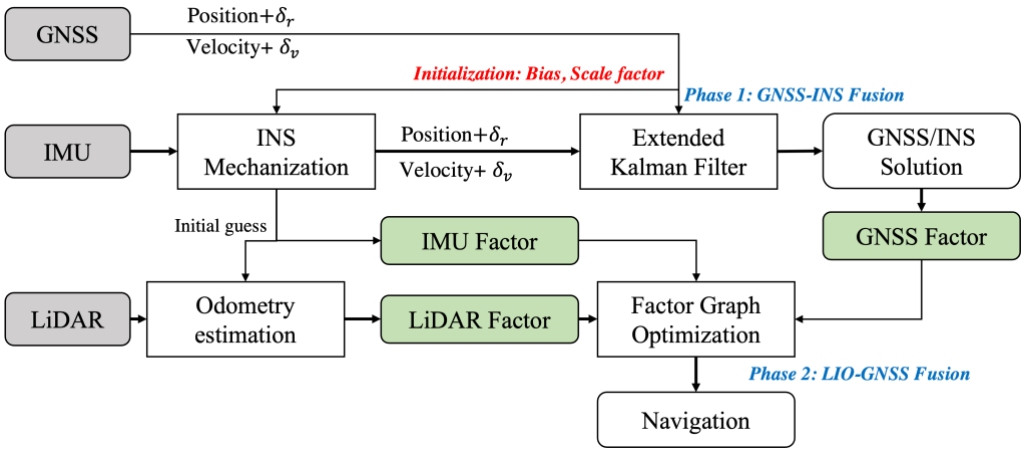

Figure 1. The overview of the proposed solution.

IMU and LiDAR to achieve precise and resilient positioning in urban canyons. Specifically, the first phase of GNSS-INS fusion leverages the EKF to integrate the GNSS positioning with IMU mechanization for the initial positioning. The subsequent LIO-GNSS fusion phase employs a LIO odometry which is estimated via a scan-to-map LiDAR odometry estimation, where the initial guess is derived from IMU mechanization. The global positioning is then estimated via a tightly coupled FGO framework that optimizes factors of LiDAR odometry, IMU mechanization, and the GNSS/INS integration factor. The contributions of this paper can be summarized as following,

(1). Introduction of a Two-Phase Sensor Fusion (TPSF) strategy that enhances navigation precision and system robustness in urban canyon environments.
(2). Implementation of the TPSF strategy, which incorporates stages of GNSS-INS fusion and LIO-GNSS fusion, hierarchically estimating the global positioning.
(3). Comprehensive evaluation and results analysis using an urban trajectory using a real-world urbanized dataset, demonstrating the evaluation analysis are implemented through two urbanized trajectories using a real-world dataset, demonstrating the robustness of the proposed solution.

2. Proposed method

2.1 Overview

The framework of the TPSF strategy introduced in this paper is shown in Figure 1. This strategy is comprised of four primary stages: INS mechanization, GNSS-INS integration via an EKF, estimation of LiDAR-Inertial odometry, and LIO-GNSS fusion. Inputs are comprised of GNSS positioning solutions obtained from a low-cost receiver, IMU measurements and the point clouds from a LiDAR. To maintain computational efficiency, keyframe selection is employed, prioritizing LiDAR frames that exhibit the most pronounced geometric features, as outlined by (Shan et al., 2020). INS mechanization processes raw IMU measurements to deduce relative poses, which also serve as initial guess for LiDAR odometry. The details of this process are expounded in the foundational works (Forster et al., 2017; Shan et al., 2021).

2.2 Coordinate and frame definition

We establish the following notations and coordinate frameworks for clarity in our methodological discourse. The local world coordinate system, denoted as $\{W(X^{ENU}, Y^{ENU}, Z^{ENU})\}$ is firstly defined aligning the East, north, and up (ENU) convention. In this coordinate, the X-axis is oriented eastward, the Y-axis northward, and the Z-axis upward. The ENU is determined by the global position given by the first fixed GNSS location. Local sensor frame including LiDAR coordinate system $\{L(X^L, Y^L, Z^L)\}$ and IMU body frame $\{B(X^B, Y^B, Z^B)\}$ are defined, which are affixed to their respective sensors.

Furthermore, we assume that the timestamps are synchronized for sensors, with timestamps $T\{t_1, t_2, .., t_k\}$, and the relative transformation matrix are well calculated, which defined the translation and rotation from sensors frame to body frame $[T_B^{sensor}, R_B^{sensor}]$.

2.3 IMU pre-integration

In this study, IMU pre-integration is implemented to estimate the IMU pre-integration factor. The raw IMU measurements can be represented as,

$$\hat{a}_t = a_t + b_{a_t} + R_t^W g^W + n_a \quad (1)$$

$$\hat{\omega}_t = \omega_t + b_{\omega_t} + n_\omega \quad (2)$$

where $\hat{a}_t$ and $\hat{\omega}_t$ are the raw measurements of the gyroscope and the accelerometer, while b and n represent the bias and additive noises. R_t^W is the rotation matrix at each timestamp. The IMU pre-integration can be calculated between timestamp $k-1$ and k, as following Equation (3),

$$\begin{aligned} \alpha_{b_k}^{b_{k-1}} &= \iint_{t\in[t_{k-1},t_k]} R_t^W(\hat{a}_t - b_{a_t})dt^2 \\ \beta_{b_k}^{b_k-1} &= \int_{t\in[t_{k-1},t_k]} R_t^W(\hat{a}_t - b_{a_t})dt \\ \gamma_{b_k}^{b_{k-1}} &= \int_{t\in[t_{k-1},t_k]} \tfrac{1}{2}\Omega(\hat{\omega}_t - b_{w_t})\gamma_t^{b_k}dt \end{aligned} \quad (3)$$

where $\Omega(\omega) = \begin{bmatrix} -\lfloor\omega\rfloor_\times & \omega \\ -\omega^T & 0 \end{bmatrix}$, $\lfloor\omega\rfloor_\times = \begin{bmatrix} 0 & -\omega_z & \omega_y \\ \omega_z & 0 & -\omega_x \\ -\omega_y & \omega_x & 0 \end{bmatrix}$

The IMU factor can be calculated as following:

$$\begin{bmatrix} \delta\dot{\alpha}_t^{b_k} \\ \delta\dot{t}_t^{b_k} \\ \delta\dot{\theta}_t^{b_t} \\ \delta\dot{b}_{a_t} \\ \delta\dot{b}_{w_t} \end{bmatrix} = \begin{bmatrix} 0 & I & 0 & 0 & 0 \\ 0 & 0 & -R_t^W[\hat{a}_t - b_{a_t}]_\times & -R_t^W & 0 \\ 0 & 0 & -[\hat{w}_t - b_{w_t}]_\times & 0 & -I \\ 0 & 0 & 0 & 0 & 0 \\ 0 & 0 & 0 & 0 & 0 \end{bmatrix} \begin{bmatrix} \delta\alpha_t^{b_t} \\ \delta\beta_t^{b_k} \\ \delta\theta_t^{b_k} \\ \delta b_{a_a} \\ \delta b_{w_t} \end{bmatrix} + \begin{bmatrix} 0 & 0 & 0 & 0 \\ -R_t^W & 0 & 0 & 0 \\ 0 & -I & 0 & 0 \\ 0 & 0 & I & 0 \\ 0 & 0 & 0 & I \end{bmatrix} \begin{bmatrix} n_a \\ n_w \\ n_{b_a} \\ n_{b_w} \end{bmatrix} \quad (4)$$

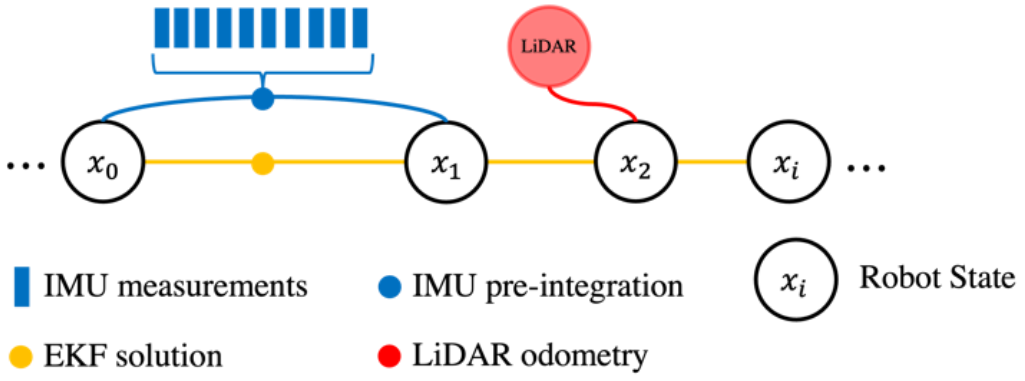

Figure 2. The structure of factor graph optimization.

2.4 LiDAR-Inertial Odometry (LIO)

In this section, LiDAR-Inertial odometry is estimated via scan-to-map matching when a new LiDAR frame is available. The first step is to extract the edge points and planar points by calculating and sorting the smooth value, following Equation (5) (Zhang and Singh, 2014),

$$s_i = \frac{1}{\|S\|}\left\|\sum_{j=1,j\neq i}^{S}(X_i^L - X_j^L)\right\| \quad (5)$$

where the s_i is the roughness of the point, while S denotes the surrounding local region of the center point X_i^L. The X_i^L will be classified as an edge point $F_{e,k}^L$ when the s_i is larger than a pre-defined threshold δ. Otherwise, the center point will be classified as a planar point $F_{p,k}^L$. Subsequently, the set of feature points is composed of the planar points and edge points.

Using the IMU pre-integration as initial guess, the relative transformation matrix can be estimated by minimizing the corresponding featured point set, which can be formulated as Equation (6),

$$\mathrm{m}_{k-1,B}^{k,B} = \rho(R_B^L(\mathrm{F}_k\{\mathrm{F}_{p,k}^L, \mathrm{F}_{e,k}^L\}, \mathrm{F}_{k-1}\{\mathrm{F}_{p,k-1}^L, \mathrm{F}_{e,k-1}^L\})) \quad (6)$$

where ρ denotes the distance minimization operation, while $\mathrm{m}_{k-1,B}^{k,B}$ is the calculated distance.

By solving the linear minimization process of $\mathrm{m}_{k-1,B}^{k,B}$, the relative transformation matrix of LIO factor can be represented as Equation (7),

$$\Delta\mathrm{T}_{k-1,k} = \mathrm{T}_{k-1}^{\mathrm{T}}\mathrm{T}_k \quad (7)$$

where $\Delta\mathrm{T}_{k-1,k}$ represents the relative LiDAR-Inertial odometry.

2.5 Fusion Stage 1: GNSS/INS Fusion

In this research, the EKF is implemented to fuse the data from the GNSS positioning solution and the INS mechanization derived from a 6-axis IMU, employing a loosely coupled sensor fusion strategy. INS mechanization computes the relative motion state using the measurements from the IMU, which include angular rates from a gyroscope and accelerative forces from an accelerometer. The GNSS positioning are transposed into the ENU frame relative to the defined initial point.

The state x of the navigation system along with variables, is articulated in terms of position r, velocity v, and the IMU specific parameters as bias and scale factors. The state function for the system can be formulated as following,

$$\chi_k = [X_k^{ENU}, v_k^{ENU}, b_{a,k}^B, b_{g,k}^B]^T \quad (8)$$

where $X_k^{ENU} = [x_k^{ENU}, y_k^{ENU}, z_k^{ENU}]$ is the positioning of the GNSS receiver in the ENU frame at a timestamp k, and $v_k^w = [v_{x,k}^w, v_{y,k}^w, v_{z,k}^w]$ demonstrates the velocity, respectively. $b_{a,k}^B$ and $b_{g,k}^B$ denote the bias of the accelerometer and gyroscope. In this study, the first stage of GNSS-INS loosely coupled system estimate each term and finish the initialization.

A brief introduction of EKF is presented herein. A general dynamic model of EKF-based loosely coupled system can be formulated as Equation (9),

$$\mathbf{x}_k = f(\mathbf{x}_{k-1}, \mathbf{u}_k) + \mathbf{w}_{k-1} \quad (9)$$

where $\mathbf{x}_k$ represents the state vector at the timestamp k. $\mathbf{u}_k$ embodies the LiDAR measurements, including IMU measurement, and $\mathbf{w}_k$ denotes the process noise. The EKF provides an iterative means to predict and update the system state by linearizing the nonlinear state transition function around the current estimate. The $f(\mathbf{x}_{k-1}, \mathbf{u}_k)$ based on the constant-velocity model, can be represented as Equation (10),

$$f(\mathbf{x}_{k-1}, \mathbf{u}_k) = \begin{bmatrix} x_{k-1}^{\mathrm{W}} + v_{k-1,x}^{\mathrm{W}} \cdot \Delta t \\ y_{k-1}^{\mathrm{W}} + v_{k-1,y}^{\mathrm{W}} \cdot \Delta t \\ z_{k-1}^{\mathrm{W}} + v_{k-1,z}^{\mathrm{W}} \cdot \Delta t \\ v_{k-1,r,x}^{\mathrm{W}} + a_{k-1,x}^{\mathrm{W}} \cdot \Delta t \\ v_{k-1,r,y}^{\mathrm{W}} + a_{k-1,y}^{\mathrm{W}} \cdot \Delta t \\ v_{k-1,r,z}^{\mathrm{W}} + a_{k-1,z}^{\mathrm{W}} \cdot \Delta t \\ b_{a,k-1,x}^{\mathrm{B}} \\ b_{a,k-1,y}^{\mathrm{B}} \\ b_{a,k-1,z}^{\mathrm{B}} \\ b_{g,k-1,x}^{\mathrm{B}} \\ b_{g,k-1,x}^{\mathrm{B}} \\ b_{g,k-1,x}^{\mathrm{B}} \end{bmatrix} \quad (10)$$

where Δt is the time difference between the relative data.

In addition, the measurement model of the EKF can be represented as the Equation (11),

$$\boldsymbol{Z}_K = h(\boldsymbol{X}_k) + \boldsymbol{e}_k \quad (11)$$

where $\boldsymbol{Z}_K = (x_k^{GNSS}, y_k^{GNSS}, z_k^{GNSS})^T$ are the positioning measurements in the ENU frame which are converted the positioning solution from the GNSS receiver, while $\boldsymbol{e}_k$ represent the Gaussian noise along with the measurements, which can be described using a covariance matrix.

Table 1. Translational error analysis.

Dataset (ape)	Error type	EKF	GNSS-LIO-SAM	LIO	Proposed solution
Translation	STD	2.230	1.372	1.373	**1.269**
(m)	Max	8.240	5.063	5.207	**5.013**
	RMSE	3.180	2.905	3.318	**2.836**

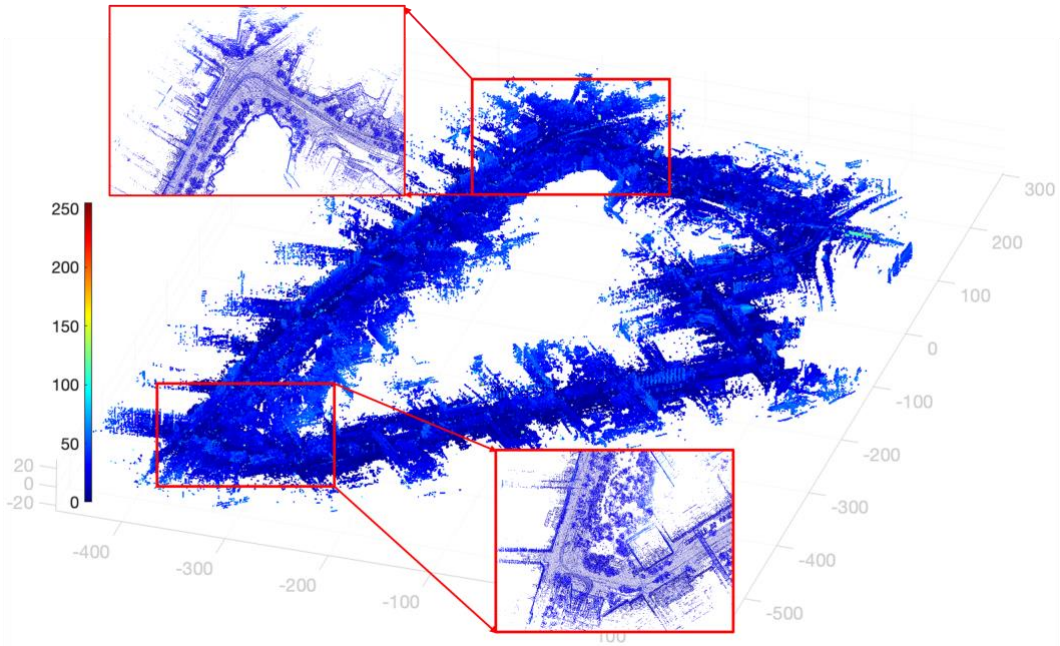

Figure 3. The 3D map results using proposed TPSF scheme.

2.6 Fusion Stage 2: LIO-GNSS/INS Fusion

In the second stage of optimization, a factor graph optimization structure is implemented to calculate the optimal state, based on the GNSS-INS positioning solution, LiDAR-Inertial Odometry, and IMU pre-integration. The structure of the FGO is shown in Figure 2. The state motion function and detailed error function are introduced as following.

The state function of the proposed factor graph optimization can be represented as Equation (12),

$$\mathrm{x} = [\mathrm{R}^{\mathrm{T}}, \mathrm{p}^{\mathrm{T}}, \mathrm{v}^{\mathrm{T}}, \mathrm{b}^{\mathrm{T}}]^{\mathrm{T}}, \quad (12)$$

where R = rotation matrix, $R \in SO(3)$
p = position vector, $p \in R^3$
v = speed
b = IMU bias

The estimation process then can be formulated as the minimization problem by solving the nonlinear least-squares problem, as Equation (13),

$$\mathrm{T}_B^{W^*} = \operatorname{argmin} \sum_{k=0,1,\ldots,K} \left(\left\| \mathrm{e}_k^{\mathrm{GNSS/INS}} \right\|^2_{\Sigma_k^{\mathrm{GNSS/INS}}} + \left\| \mathrm{e}_k^{IMU} \right\|^2_{\Sigma_k^{\mathrm{IMU}}} + \left\| \mathrm{e}_k^{LIO} \right\|^2_{\Sigma_k^{\mathrm{LIO}}} \right) \quad (13)$$

where the defined three error factors are GNSS-INS factor $\mathrm{e}_k^{\mathrm{GNSS/INS}}$, IMU pre-integration factor e_k^{IMU} and LiDAR-Inertial odometry factor e_k^{LIO}. Especially, the error function of each factor can be represented as following:

$$\left\| \mathbf{e}_k^{IMU} \right\|^2_{\Sigma_k^{LDARR}} = \left\| \left\| \mathbf{T}^W_{B,k-1}{}^{-1} \boldsymbol{T}^W_{B,k} \right\|^2 \right\|^2_{\Sigma_k^{IMU}} \quad (14)$$

$$\left\| \mathrm{e}_k^{LIO} \right\|^2_{\Sigma_k^{\mathrm{LIO}}} = \left\| \left(\mathbf{T}^{ENU}_{B,k-1}{}^{-1} \boldsymbol{T}^{ENU}_{B,k} \right) \ominus \left(\mathbf{T}^{L}_{B,k-1}{}^{-1} \boldsymbol{T}^{L}_{B,k} \right) \right\|^2_{\Sigma_k^{LIO}} \quad (15)$$

$$\left\| \mathrm{e}_k^{GNSS/INS} \right\|^2_{\Sigma_k^{\mathrm{GNSS/INS}}} = \left\| \left(\mathbf{T}^{ENU}_{B,k-1}{}^{-1} \boldsymbol{T}^{ENU}_{B,k} \right) \right\|^2_{\Sigma_k^{GNSS/INS}} \quad (16)$$

where $\|\mathbf{e}\|^2_{\sum k}$ is the error function between keyframe $k-1$ and k, while the operation $\ominus$ is the minus operation.

3. Experimental Results

3.1 Experiment details

In our study, we assess the effectiveness of the proposed TPSF strategy through a series of experiments conducted along an urban trajectory characterized by dense, urban canyon-like environments (Hsu et al., 2021). This trajectory was specifically chosen to test the robustness of the TPSF strategy under challenging urban conditions.

To rigorously evaluate the TPSF strategy, we designed a set of ablation experiments, each focusing on a different aspect of the sensor fusion process. These experiments were conducted using the Robot Operating System (ROS) on an Ubuntu Linux platform and include:

(1). GNSS/INS Integration via Extended Kalman Filter (EKF): This experiment tests the baseline performance of integrating Global Navigation Satellite System (GNSS) data with Inertial Navigation System (INS) outputs using an EKF.
(2). Direct GNSS Positioning with Factor Graph Optimization (FGO): Here, GNSS positioning is fixed and directly fused with

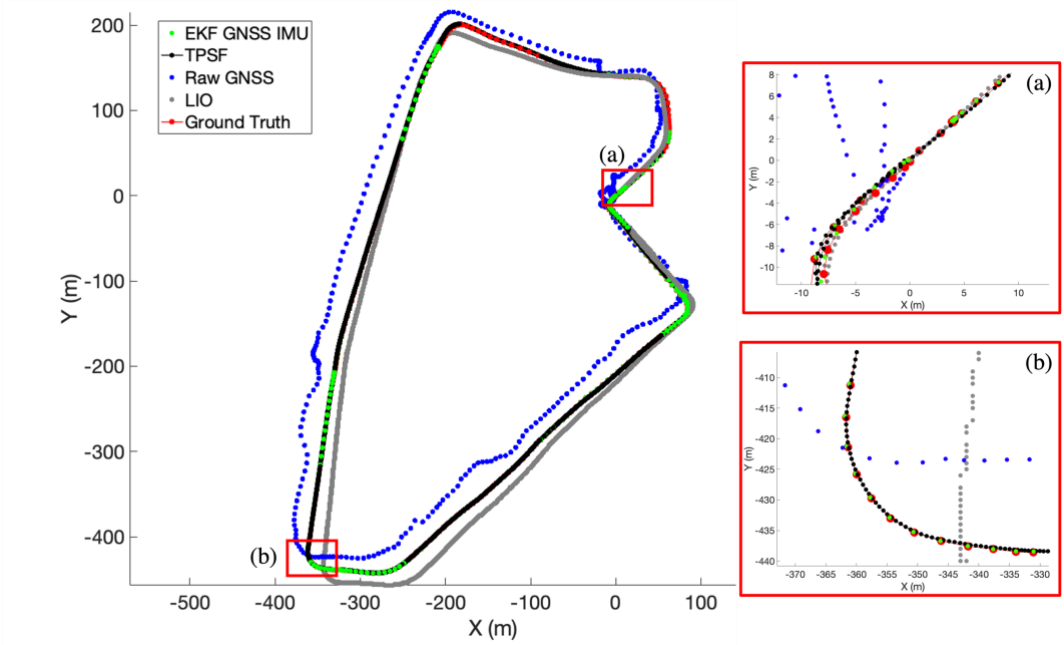

Figure 4. The estimated trajectories and ground truth.

LiDAR-Inertial Odometry (LIO) and IMU pre-integration factors using FGO, bypassing the EKF step.
(3) Lidar-Inertial Odometry Optimization via FGO: This setup focuses on optimizing the Lidar-Inertial odometry factor with FGO, evaluating the performance improvement when LIO data is directly optimized.

The performance of the TPSF strategy across these experiments is quantitatively evaluated based on translational errors, employing the following metrics:

STD (Standard Deviation): Measures the variability or dispersion of the error distribution.
RMSE (Root Mean Square Error): Provides a measure of the magnitude of the error, combining both the variance and the bias of the predictions.
MAX (Maximum Error): Identifies the worst-case error scenario, offering insights into the extreme outliers in the data.

These metrics collectively offer a comprehensive view of the TPSF strategy's accuracy, reliability, and robustness in navigating complex urban environments.

3.2 Mapping results and performance evaluation

Figure 3 illustrates the 3D mapping results achieved with the proposed TPSF solution in a complex urban environment, characterized by dense structures and dynamic objects. The detailed zoom-in views highlight the superior structural detail and clearer delineation of building boundaries achieved by the TPSF solution. This enhancement is attributed to the innovative two-stage optimization and SLAM (Simultaneous Localization and Mapping) strategy, which notably mitigates drift errors, particularly in the z-direction.
Table 1 presents the outcomes of our ablation study, comparing the performance of the proposed TPSF solution against baseline methods in terms of translational errors. The results underscore the TPSF's effectiveness in significantly reducing errors. Notably, the TPSF solution demonstrates a marked improvement

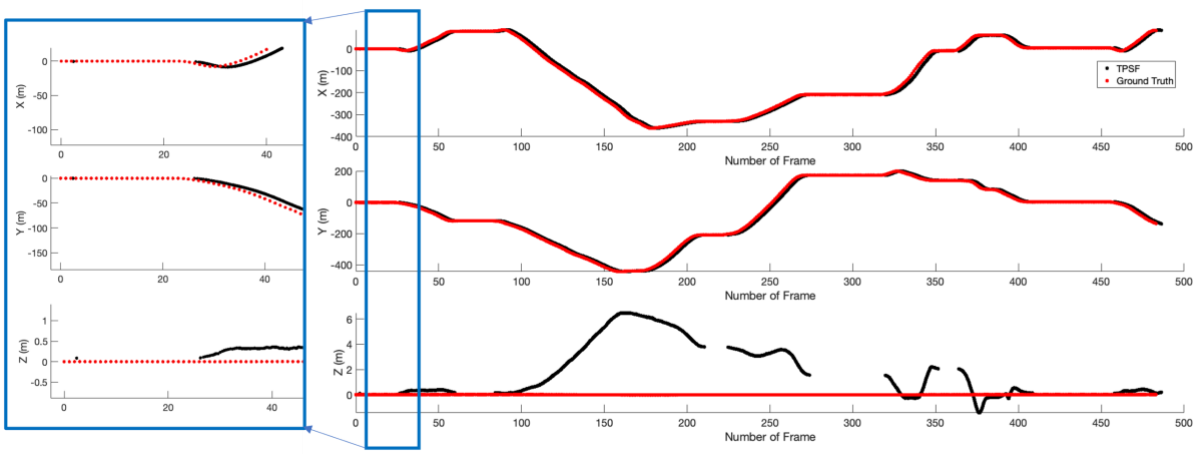

Figure 5. Translational errors in different directions.

in translational RMSE over conventional EKF and LIO approaches. Furthermore, when compared to methods utilizing GNSS positioning as a constraint, the TPSF solution achieves superior performance, reducing the translational STD from 1.4 m to 1.3 m, showcasing its robustness and accuracy.

Figures 4 and 5 further validate the TPSF's performance through visual comparison of estimated trajectories and translational differences across three axes. Figure 4(a) reveals the TPSF's capability to maintain a stable initial position relative to other solutions. A closer examination of a significant turn in the trajectory (Figure 4(b)) demonstrates the TPSF's ability to counteract drift, maintaining accuracy even in the presence of substantial rotational changes. The translational trajectory, depicted by black points, closely aligns with the ground truth (red points), highlighting the precision of the TPSF solution. Notably, the absence of TPSF output prior to successful initialization is indicated within a blue box, emphasizing the initialization process's critical role.

4. Conclusion and Future work

This study introduces a novel two-phase sensor fusion strategy, the TPSF, which integrates LiDAR, IMU, and GNSS data to significantly enhance SLAM robustness in challenging urban canyon environments. The TPSF employs a dual-stage approach for precise pose estimation and mapping in complex urban settings. Initially, the system leverages GNSS positioning and IMU pre-integration for system initialization and initial global positioning estimation. Subsequently, it incorporates LiDAR-Inertial odometry, further IMU pre-integration, and GNSS-INS data within a factor graph optimization framework to refine global pose estimation and mapping.

Distinct from conventional single-stage sensor fusion approaches, the TPSF presents two primary advantages: (1) It enables early estimation of IMU parameters, significantly enhancing the performance of both LIO and IMU pre-integration. (2) It effectively mitigates the risk of the system converging to local minima, a common challenge in sensor fusion applications, particularly under conditions of signal degradation.

However, the study acknowledges a limitation in its assumption that no outliers in relative pose estimation occur during the second stage of optimization. The presence of significant outliers, especially in the z-direction, can lead to considerable drift if LiDAR odometry estimates converge to local minima. Addressing this, future work will focus on enhancing outlier detection and removal mechanisms to bolster the SLAM system's resilience and reliability.

Acknowledgements

This research has been supported by funding of Prof. Naser El-Sheimy from NSERC CREATE and Canada Research Chairs programs.

References

Ai, M., Asl Sabbaghian Hokmabadi, I., Elhabiby, M., Moussa, M., Zekry, A., Mohamed, A., El-Sheimy, N., 2023. Lidar-Inertial Localization With Ground Constraint in a Point Cloud Map. ISPRS Ann. Photogramm. Remote Sens. Spat. Inf. Sci. X-1/W1-202, 613–619. https://doi.org/10.5194/isprs-annals-x-1-w1-2023-613-2023

Ai, M., Luo, Y., El-Sheimy, N., 2022. Surround Mask Aiding GNSS/LiDAR SLAM for 3D Mapping in the Dense Urban Environment. Proc. 35th Int. Tech. Meet. Satell. Div. Inst. Navig. (ION GNSS+ 2022) 2011–2019. https://doi.org/10.33012/2022.18550

Chiang, K.W., Tsai, G.J., Chang, H.W., Joly, C., EI-Sheimy, N., 2019. Seamless navigation and mapping using an INS/GNSS/grid-based SLAM semi-tightly coupled integration scheme. Inf. Fusion 50, 181–196. https://doi.org/10.1016/j.inffus.2019.01.004

Chiang, K.W., Tsai, G.J., Chu, H.J., El-Sheimy, N., 2020. Performance Enhancement of INS/GNSS/Refreshed-SLAM Integration for Acceptable Lane-Level Navigation Accuracy. IEEE Trans. Veh. Technol. 69, 2463–2476. https://doi.org/10.1109/TVT.2020.2966765

Forster, C., Carlone, L., Dellaert, F., Scaramuzza, D., 2017. On-Manifold Preintegration for Real-Time. IEEE Trans. Robot. 33, 1–21.

Liu, X., Wen, W., Hsu, L.T., 2023. GLIO: Tightly-Coupled GNSS/LiDAR/IMU Integration for Continuous and Drift-free State Estimation of Intelligent Vehicles in Urban Areas. IEEE Trans. Intell. Veh. PP, 1–12. https://doi.org/10.1109/TIV.2023.3323648

Moussa, M., Moussa, A., Salib, A., El-Sheimy, N., 2021. Mass Flow Meter and Vehicle Information DR Land Vehicles Navigation System in Indoor Environment 1–5. https://doi.org/10.1109/iccspa49915.2021.9385713

Shan, T., Englot, B., Meyers, D., Wang, W., Ratti, C., Rus, D., 2020. LIO-SAM: Tightly-coupled lidar inertial odometry via smoothing and mapping. IEEE Int. Conf. Intell. Robot. Syst. 5135–5142. https://doi.org/10.1109/IROS45743.2020.9341176

Shan, T., Englot, B., Ratti, C., Rus, D., 2021. LVI-SAM: Tightly-coupled Lidar-Visual-Inertial Odometry via Smoothing and Mapping. Proc. - IEEE Int. Conf. Robot. Autom. 2021-May, 5692–5698. https://doi.org/10.1109/ICRA48506.2021.9561996

Wang, G., Gao, S., Ding, H., Zhang, H., Cai, H., 2021. LIO-CSI: LiDAR inertial odometry with loop closure combined with semantic information. PLoS One 16, 1–18. https://doi.org/10.1371/journal.pone.0261053

Wen, W., Pfeifer, T., Bai, X., Hsu, L.T., 2021. Factor graph optimization for GNSS/INS integration: A comparison with the extended Kalman filter. Navig. J. Inst. Navig. 68, 315–331. https://doi.org/10.1002/navi.421

Zhang, J., Singh, S., 2014. LOAM: Lidar Odometry and Mapping in Real-time, Robotics: Science and Systems, . Robot. Syst. 2, 9–17.